Nigerian Journal of Theoretical and Environmental Physics (NJTEP)
ISSN Print: 3026-9601
ISSN Online: 1597-9849
DOI: https://doi.org/10.62292/njtep.v3i4.2025.102
Volume 3(4), December 2025

Thermo-Magnetic properties of Two-Dimensional Non-Relativistic Schrödinger Equation for the Attractive Radial Potential under External Magnetic and Aharonov-Bohm Flux Fields

***[1]Mohammed H. Imrana, [2]Adam Z. Ngari, [3]Peter B. Teru, [4]Gyobe, A. M., [5]Ndom B. Ndom, [1]Jibrin A. Yabagi and [1]Babakatcha Ndanusa**

[1]Department of Physics, Ibrahim Badamasi Babangida University Lapai, Niger State, Nigeria
[2]Department of Physics, Nigerian Army University Biu, Borno State, Nigeria
[3]Department of Physics, University of Maiduguri, Borno State, Nigeria
[4]Department of Physics, Nigeria Maritime University of Okeronkoko
[5]Air force Institute of Technology, Kaduna, Nigeria

*Corresponding author's email: mimrana507@gmail.com

ABSTRACT

We investigate the thermo-magnetic properties of the Attractive Radial Potential (ARP) for a particle moving in two-dimensional non-relativistic Schrödinger equation subjected to an external magnetic field and Aharonov-Bohm (AB) flux. Analytical solution for the energy eigenvalues and wavefunctions were obtained in a closed form via the Nikiforov-Uvarov Functional Analysis (NUFA) method. We derived the partition function by analyzing the system as a canonical ensemble to obtain the expressions for the thermodynamic quantities which include the free energy, entropy, specific heat capacity and internal energy. Our results show a decrease in the energy spectrum when the AB flux and magnetic fields are increased. At low temperatures, specific heat capacity shows a peak anomaly, while Helmholtz free energy and entropy exhibit temperature dependence. We also observed that AB flux and magnetic field influence both magnetization and magnetic susceptibility and exhibit both paramagnetic and diamagnetic behavior. The findings provide valuable insights into in molecular physics applications.

Keywords:
Thermo-magnetic properties,
Attractive radial potential,
Non-relativistic solution,
External magnetic field,
Aharanov-Bohm flux.

INTRODUCTION

The various potential models with in the solution of wave equations is important in the study of physics, as their solutions provide essential imformation into physical systems and phenomena (Greiner 2000; Landau 1977; Schiff 1995; Dirac 1958; Louis et al., 2018). The understanding of particle behavior under different conditions can be utilized through these solutions. Numerous potential models to study various physical interactions have been introduced and employed by researchers over the years (Abu-Shady & Fath-Allah 2023; Serrano et al., 2010). These potentials are dependent of inter-particle distance and specific potential parameters that govern the nature of the interaction (Khordad & Mirhosseini 2015). But, a limited number of these potential models, such as the harmonic oscillator potential, the Coulomb potential and Kratzer potential, can give exact analytical solutions (Servatkhah et al., 2020). Where exact solutions cannot be utilize for nonzero angular momentum quantum numbers, the Greene and Aldrich method approximation techniques (Greene & Aldrich 1976) or the Pekeris approximation (Pekeris 1934) are employed. To derive the equation for exponential type potentials in two-dimensional system several analytical techniques have been utilized. These include the factorization method (Dong 2007; Ikot et al., 2020), the Nikiforov-Uvarov (NU) method (Nikiforov & Uvarov 1988), the asymptotic iteration method (AIM) (Çiftçi et al., 2005; Bayrak et al., 2007), the NU functional analysis (NUFA) method (Ikot et al., 2021), exact quantization rules (Qiang & Dong 2010; Serrano et al., 2011), supersymmetric quantum mechanics, and the extended Nikiforov-Uvarov (ENU) approach (Karayer 2020; Karayer et al., 2015).

The Attractive Radial Potential (ARP), is one of the interesting potential model introduced by Williams and Poulios, (1993) given in the form:

$$V(r) = \frac{a_0 e^{-2\alpha r} + b_0 + c_0 e^{2\alpha r}}{e^{2\alpha r}(1-e^{-2\alpha r})^2} \quad (1)$$

Researchers have explored this exponential-type potential with four parameters under both relativistic and non-relativistic frameworks (Eshghi & Hamzavi 2012). The bound-state solutions of these potential, as well as its quantum information measures such as information energy, Rényi entropy, and Tsallis entropy, and scattering phase shifts in higher dimensions has been explored from previous research (Okorie et al., 2021). Notably, the Attractive Radial Potential (ARP) exhibit inter-dimensional degeneracy symmetry in the scattering phase shifts (Okorie et al., 2021).

In quantum mechanics, the external fields have played a fundamental role to influence the energy spectra through the effects such as Zeeman splitting and the Stark effect (Ikot et al., 2020). The degeneracies or induce spectral shifts, significantly altering a system's behavior can be lift by these fields. Researchers recently explored the impact of magnetic and AB flux fields in various quantum systems, such as the position-dependent mass Schrödinger equations (Ikot et al., 2020), and diatomic molecules under Aharonov-Bohm (AB) flux and magnetic fields (Edet et al., 2020). It is of these developments that, this research investigates the influence of AB flux and magnetic fields on the Attractive Radial Potential (ARP) model.

However, investigating the thermal and magnetic properties of quantum systems has attracted significant attention by researchers (Okorie et al., 2019; Okorie et al., 2020). Properties such as entropy, internal energy, free energy, magnetization, and susceptibility provide crucial insights into system behavior under different conditions. While previous studies have examined these properties for various potentials (Ikhdair & Falaye 2014), there has been no comprehensive investigation of the impact of magnetic and AB fields on an attractive radial potential.

In this work, we extend the study of the ARP model by investigating its thermo-magnetic properties influenced by magnetic field and AB flux field. Applying the Nikiforov-Uvarov functional analysis (NUFA) method, Closed-form solutions for the energy spectrum equation and the corresponding wavefunctions are derived. We further apply the energy spectrum to analyze the behavior of thermo-magnetic quantities, including the partition function, entropy, internal energy, free energy and specific heat capacity.,

Solution of Non-relativistic Schrödinger equation with ARP model subject to AB flux and magnetic fields

Let's assume a non-relativistic system of particles to move on a plane under the effect of ARP subject to both external magnetic field and Aharonov-Bohm (AB) flux field, perpendicular to the plane. Then, the stationary Schrödinger equation to investigate the system in polar coordinates takes the form (Eshghi et al., 2017);

$$\frac{\vec{P}^2}{2\mu}\psi(r,\phi) = [E_{nm} - V(r)]\psi(r,\phi) \quad (2)$$

where E_{nm} denote the energy eigenvalue, μ represent the reduced mass. This work is aimed to study the physical characteristic of the system using ARP as given in Equation (1). Accordingly, with this assumption, the momentum operator for the charged particle needs to be altered, and we apply a minimal coupling of a four-vector to the operator in the following manner:

$$\vec{P} = \left(i\hbar\vec{\nabla} + \frac{e}{c}\vec{A}\right) \quad (3)$$

In order to incorporate both the magnetic and Aharonov-Bohm flux fields, the vector potential is written as a combination of two azimuthal terms. $\vec{A} = \vec{A}_1 + \vec{A}_2$. Let's assumed

$$\vec{A}_1 = \left(\frac{Be^{-2\alpha r}}{1-e^{-2\alpha r}}\right)\hat{\phi} \quad (4)$$

This gives the external magnetic field only with the azimuthal component by the well-known formula $\vec{\nabla} \times \vec{A}_1 = \vec{B}$. To indicate Aharonov-Bohm (AB) flux φ_{AB}. We use

$$\vec{A}_2 = \left(\frac{\varphi_{AB}}{2\pi r}\right)\hat{\phi} \quad (5)$$

This satisfies the condition $\vec{\nabla} \times \vec{A}_2 = 0$ and $\vec{\nabla} \cdot \vec{A}_2 = 0$. Henceforth, the total vector potential can be expressed as reported by (Falaye et al., 2016; Edet et al., 2020)

$$\vec{A} = \left(0, \frac{Be^{-2\alpha r}}{(1-e^{-2\alpha r})} + \frac{\Phi_{AB}}{2\pi r}\right)\hat{\phi} \quad (6)$$

For stationary Schrödinger equation to be solved the eigenfunction in the cylindrical coordinates is assumed using the ansatz;

$$\psi(r,\phi) = \frac{1}{\sqrt{2\pi r}} e^{im\phi} R_{nm}(r,\phi) \quad (7)$$

where m gives the magnetic quantum number and ϕ is the azimuth angle. With equation (1), (3), (6) and (7) into equation (2). The radial second-order differential equation is obtained:

$$R''(r) + \frac{2\mu}{\hbar^2}\left[E_{nm} - V_{eff}(r,\omega_B,\zeta_{AB})\right]R(r) = 0 \quad (8)$$

where $V_{eff}(r,B,\Phi_{AB})$ represent the effective potential, expressed as:

$$V_{eff}(r,\omega_B,\zeta_{AB}) = V(r) - \frac{\hbar\omega_B(m+\zeta_{AB})e^{-2\alpha r}}{(1-e^{-2\alpha r})r} + \frac{(\mu\omega_B^2)e^{-4\alpha r}}{2(1-e^{-2\alpha r})^2} + \frac{\hbar^2\left((m+\zeta_{AB})^2 - \frac{1}{4}\right)}{(2\mu)r^2} \quad (10)$$

where $\zeta_{\mathrm{AB}} = \frac{\varphi_{AB}}{\varphi_0}$, with $\varphi_0 = \frac{2\pi\hbar c}{e} = \frac{hc}{e}$; $\tau = -\frac{e}{c}$, and $\omega_B = -\frac{B\tau}{\mu}$ being the cyclotron frequency. To take care of centrifugal term we employed the Greene - Aldrich approximation scheme (Greene & Aldrich 1976), that valid only for small screening parameter α.

$$\frac{1}{r^2} \approx \frac{4\alpha^2}{(1-e^{-2\alpha r})^2}; \quad \frac{1}{r} \approx \frac{2\alpha}{(1-e^{-2\alpha r})} \quad (11)$$

Let consider coordinate transformation of the form$x = e^{-2\alpha r}$, to bypass the centrifugal term and performing some straightforward algebraic simplification, equation (8) reduced to:

$$\frac{d^2R(x)}{dx^2} + \frac{(1-x)}{x(1-x)}\frac{dR(x)}{dx} + \frac{1}{x^2(1-x)^2}\begin{bmatrix} -(\varepsilon_{nm} + \delta_0 + \eta_1)x^2 \\ +(2\varepsilon_{nm} - \delta_1 - \eta_0)x \\ -(\varepsilon_{nm} + \delta_2 + \eta_2) \end{bmatrix} R(x) = 0 \quad (12)$$

The following dimensionless notation is introduced for simplification:

$$\varepsilon_{nm} = -\frac{\mu E_{nm}}{2\hbar^2\alpha^2}, \delta_0 = \frac{\mu a_0}{2\hbar^2\alpha^2}, \delta_1 = \frac{\mu b_0}{2\hbar^2\alpha^2}, \delta_2 = \frac{\mu c_0}{2\hbar^2\alpha^2},$$
$$\eta_0 = \frac{\mu\omega_B(m+\zeta_{AB})}{\hbar\alpha}, \eta_1 = \frac{\mu^2\omega_B^2}{4\hbar^2\alpha^2}, \eta_2 = (m+\zeta_{AB})^2 - \frac{1}{4} \quad (13)$$

To solve equation (12) we define the ansatz:

$$R(x) = x^{\lambda}(1-x)^{\sigma}f(x) \quad (14)$$

The following dimension is used for the NUFA method as reported by Ikot et al. (2021)

$$\lambda = \sqrt{\varepsilon_{nm} + \delta_2 + \eta_2} \quad (15)$$

$$\sigma = \frac{1}{2} + \sqrt{\frac{1}{4} + \Lambda_\delta + \Lambda_\eta} \quad (16)$$

where

$$\Lambda_\delta = \delta_0 + \delta_1 + \delta_2;\ \Lambda_\eta = \eta_0 + \eta_1 + \eta_2 \quad (17)$$

The energy eigenvalue for the ARP subject to magnetic and an AB field is derived as:

$$\varepsilon_{nm} = -\delta_2 - \eta_2 + \left[\frac{\delta_0 - \delta_2 + \eta_1 - \eta_2 - \left(n + \frac{1}{2} + \sqrt{\frac{1}{4} + \Lambda_\delta + \Lambda_\eta}\right)^2}{2\left(n + \frac{1}{2} + \sqrt{\frac{1}{4} + \Lambda_\delta + \Lambda_\eta}\right)}\right]^2 \quad (18)$$

Therefore, we substitute the values of the dimensionless parameters of equation (13) into equation (18); the solution of the ARP subject to magnetic and an AB flux field is obtained as:

$$E_{nm} = \frac{2\hbar^2\alpha^2}{\mu}\left((m+\zeta_{AB})^2 - \frac{1}{4}\right) + c_0 - \frac{2\hbar^2\alpha^2}{\mu}\left[\frac{\frac{\mu}{2\hbar^2\alpha^2}(a_0 - c_0) + \frac{\mu^2\omega_B^2}{4\hbar^2\alpha^2} - (m+\zeta_{AB})^2 - \frac{1}{4} - (n+\widehat{K})^2}{2(n+\widehat{K})}\right]^2 \quad (19)$$

where $\widehat{K} = \frac{1}{2} + \sqrt{(m+\zeta_{AB})^2 + \frac{\mu}{2\hbar^2\alpha^2}(a_0 + b_0 + c_0) + \frac{2\mu\omega_B(m+\zeta_{AB})}{\hbar\alpha} + \frac{\mu^2\omega_B^2}{4\hbar^2\alpha^2}}$ (20)

In d-dimensional non-relativistic energy solutions when$m = 0$, where $l$is the rotational quantum number, equation (19) reduced to:

$$E_{nl} = c_0 - \frac{2\hbar^2\alpha^2}{\mu}\left[\frac{\frac{\mu}{2\hbar^2\alpha^2}(a_0 - b_0) - \left(n + \frac{1}{2} + \sqrt{(1+4\upsilon) + \frac{\mu}{2\hbar^2\alpha^2}(a_0 + b_0 + c_0)}\right)^2}{2\left(n + \frac{1}{2} + \sqrt{(1+4\upsilon) + \frac{\mu}{2\hbar^2\alpha^2}(a_0 + b_0 + c_0)}\right)}\right]^2 \quad (21)$$

where

$$\upsilon = \frac{(D-1)(D-3)}{4} + l(l+D-2) \quad (22)$$

Equation (21) is similar with equation (15) of Okorie et al. (2021).

The corresponding unnormalized wave function is obtained using equation (14), (15) and (16):

$$R_{nm}(x) = N_{nm}x^{\sqrt{\varepsilon_{nm}+\delta_2+\eta_2}}(1-x)^{\frac{1}{2}+\sqrt{\frac{1}{4}+\Lambda_\delta+\Lambda_\eta}} \times \left({}_2F_1(-n, n+2(\lambda+\sigma); 2\lambda+1; x)\right) \quad (23)$$

where N_{nm} gives the normalization constant and ${}_2F_1(-n, n+2(\lambda+\sigma); 2\lambda+1; x)$ represent the hypergeometric function.

Thermo magnetic Properties of ARP Model

The thermo-magnetic properties of the ARP system are analyzed through the evaluation of its partition function. It is well established that, within the canonical ensemble framework, the partition function is obtained by summing over all possible vibrational energy levels accessible to the system (Servatkhah et al., 2020);

$$Z(\beta) = \sum_{n=0}^{n_{max}\Sigma} e^{-\beta E_{nm}}, \beta = \frac{1}{k_B T} \quad (24)$$

where k_B = Boltzmann constant and T is absolute temperature, E_{nm} is the energy on the nth bound state. Equation (19) can take the form;

$$E_{nm} = \Delta_1 - \frac{2\hbar^2\alpha^2}{\mu}\left[\frac{\Delta_2-(n+\tilde{K})^2}{2(n+\tilde{K})}\right] \quad (25)$$

$$\Delta_1 = \frac{2\hbar^2\alpha^2}{\mu}\left((m+\zeta_{AB})^2 - \frac{1}{4}\right) + c_0$$

$$\Delta_2 = \frac{\mu}{2\hbar^2\alpha^2}(a_0 - c_0) + \frac{\mu^2\omega_B^2}{4\hbar^2\alpha^2} - (m+\zeta_{AB})^2 - \frac{1}{4} \quad (26)$$

Put equation (25) into equation (24) we obtain

$$Z(\beta) = \sum_{n=0}^{n_{max}\Sigma} e^{-\beta\left[\Delta_1 - \frac{2\hbar^2\alpha^2}{\mu}\left(\frac{\Delta_2-(n+\tilde{K})^2}{2(n+\tilde{K})}\right)^2\right]} \quad (27)$$

where gives the maximum value of the quantum number obtaining by setting the derivative of equation (25) to zero.

Classically, we replace the summation of equation (27) with an integral of the form, (28)

$$\hat{Y} = \frac{\hbar^2\alpha^2\Delta_2^2}{4\mu}, \hat{X} = \frac{\hbar^2\alpha^2\Delta_2}{\mu} + \Delta_1, \hat{J} = \frac{\hbar^2\alpha^2}{4\mu} \quad (29)$$

Mathematica software is used to evaluate equation (28) and the expression of the partition function becomes:

$$Z(\beta) = -\frac{e^{-\hat{X}\beta-2\theta}\sqrt{\pi}n\mathrm{Erf}[(\Omega_+e^{4\theta}-\Omega_-)-(\Pi_+e^{4\theta}+\Pi_-)]_{max}}{4\sqrt{-\hat{J}\beta}} \quad (30)$$

where $\theta = \sqrt{-\hat{Y}\beta}\sqrt{-\hat{J}\beta}$

$$\Omega_+ = \frac{\sqrt{-\hat{Y}\beta}}{2\hat{K}} + 2\hat{K}\sqrt{-\hat{J}\beta}\,; \Omega_- = \frac{\sqrt{-\hat{Y}\beta}}{2\hat{K}} - 2\hat{K}\sqrt{-\hat{J}\beta}$$

$$\Pi_+ = 2\hat{K}\sqrt{-\hat{J}\beta} + \sqrt{-\hat{J}\beta}n\frac{\sqrt{-\hat{Y}\beta}}{2\hat{K}+n_{max};\hat{=}\sqrt{-\hat{J}\beta}\sqrt{-\hat{J}\beta}_{max_{max}}} \quad (31)$$

Equation (30) serves as the fundamental distribution function from which various thermodynamic and magnetic properties of the ARP system are derived. These include the free energy, internal energy, specific heat capacity, and entropy. The magnetization at finite temperatures and magnetic susceptibility at finite temperatures are also included. Furthermore, the corresponding thermodynamic and magnetic functions, as well as the magnetization and magnetic susceptibility at zero temperature, can be evaluated using the following expressions (Koscik & Okopinska 2007; Elsaid et al., 2020);

Free energy $F(\beta) = -\frac{1}{\beta} ln\, Z\,(\beta)$

Entropy $S(\beta) = -k_\beta \frac{\partial F(\beta)}{\partial \beta}$

Internal energy $U(\beta) = \frac{\partial\, ln\, Z(\beta)}{\partial \beta}$

Specific heat capacity $C_V(\beta) = k_B \frac{\partial U(\beta)}{\partial \beta}$

Magnetization at finite temperatures

$$M(\beta) = \frac{1}{\beta}\left(\frac{1}{Z(\beta)}\right)\left(\frac{\partial Z(\beta)}{\partial \beta}\right)$$

Magnetic susceptibility at finite temperatures $\chi_m(\beta) = \frac{\partial M(\beta)}{\partial \beta}$

Magnetization at zero temperature in a state (n, m) $\chi_m(\beta) = \frac{\partial M(\beta)}{\partial \beta}$

Magnetic susceptibility at zero temperature $\chi_{nm}(\omega_B, \zeta_{AB}) = \frac{\partial M(\omega_B, \zeta_{AB})}{\partial B}$

RESULTS AND DISCUSSION

In this study, we analytically solved the 2D Schrödinger equation with the Attractive Radial Potential (ARP) using the Nikiforov-Uvarov Functional Analysis (NUFA) approach. The closed-form energy spectrum and the associated unnormalized wavefunction appear in Eqs. (19) and (23). The numerical computations were performed with the following arbitrary parameter values:$a_0 = 6, b_0 = c_0 = 3, \alpha = 0.5$ and$\hbar = \mu = \tau = 1$.

Energy eigenvalue

Figures 1(a–d) present the variation of the energy eigenvalues of the Attractive Radial Potential (ARP) model as functions of the external magnetic field and Aharonov-Bohm (AB) flux field. In Figures 1(a) and 1(b), the energy eigenvalues are observed to decrease with increasing external magnetic field under varying AB flux parameters for the cases when $m = n = 0$and $m = n = 1$. Both cases reveal a consistent influence of the AB flux field on the energy spectra. Similarly, in Figures 1(c) and 1(d), the energy eigenvalues decrease as the AB flux parameter increases for different values of the external magnetic field. These cases also exhibit a uniform influence of the external magnetic field on the energy levels. Figures 2(a–d) illustrate the dependence of the ARP model's energy eigenvalues on the principal quantum number $(n)$and magnetic quantum number(m). In Figure 2(a), the energy eigenvalues decrease with increasing principal quantum number for various AB flux parameters. In Figure 2(b), a similar decreasing trend is observed as the principal quantum number increases under different external magnetic field. Furthermore, Figure 2(c) shows that the energy eigenvalues decrease as the magnetic quantum number increases for varying AB flux parameters, while Figure 2(d) indicates a comparable behavior with increasing magnetic quantum number under different external magnetic field strengths.

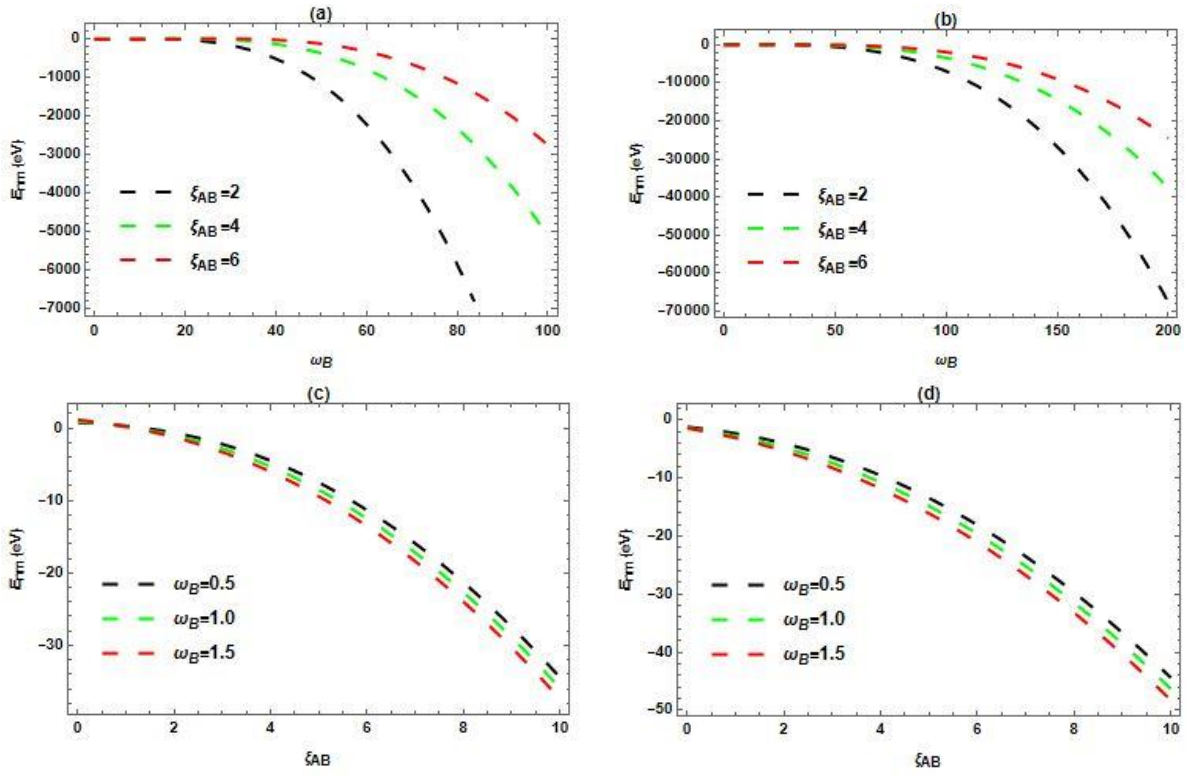

Figure 1: Plots of energy eigenvalue as a function of (a-b) External magnetic field ω_B varying $\boldsymbol{\zeta_{AB}}$ flux for m = n = 0 andφ_{AB}. (c-d) AB flux $\boldsymbol{\zeta_{AB}}$ varying ω_B for m = n = 0 andm = n = 1.

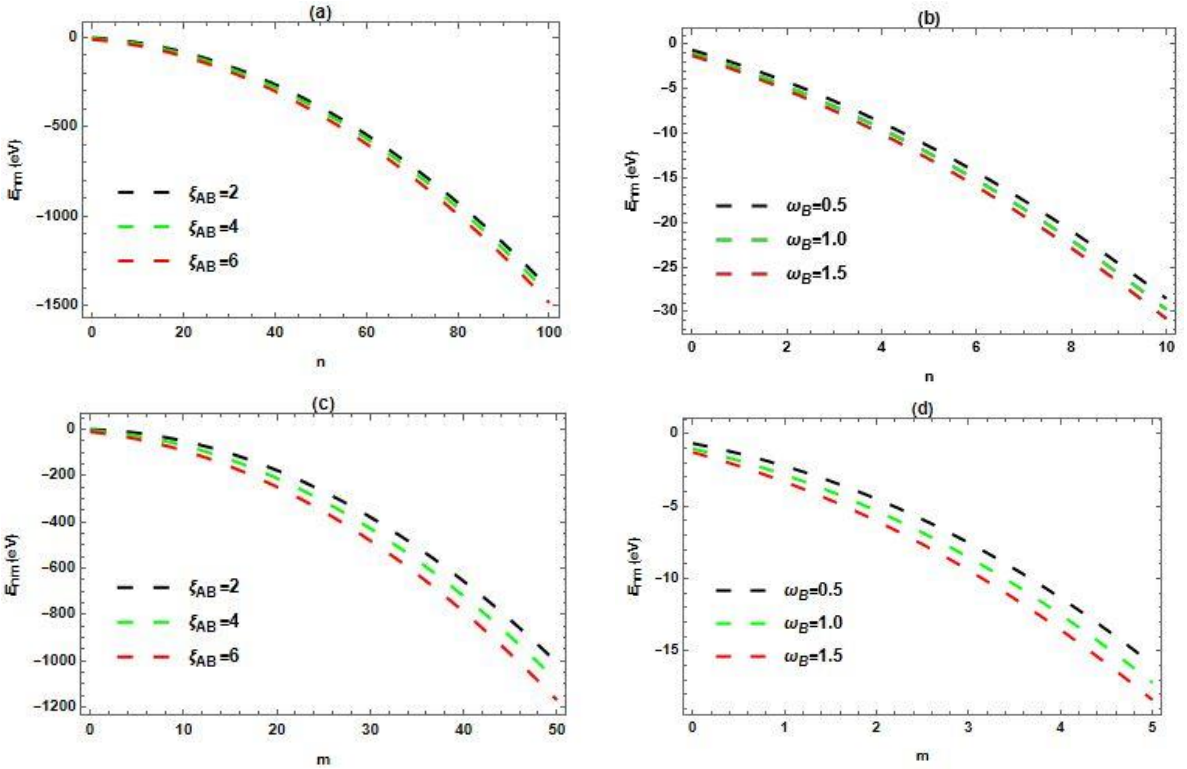

Figure 2: Plots of energy eigenvalue as a function of (a-b) Principle quantum number (n) varying ζ_{AB} andω_B. (c-d) Magnetic quantum number (m) varying ζ_{AB} and ω_B

Magnetization and Magnetic Susceptibility at Zero Temperature

In Figures 3(a–d), the magnetization of the ARP system at zero temperature under the influence of an external magnetic field and Aharonov-Bohm (AB) flux field is illustrated. Figures 3(a) and 3(b) present the variation of magnetization with respect to the external magnetic field (ω_B) for different values of the AB flux field(ζ_{AB}). It is observed that the magnetization increases monotonically as the external magnetic field (ω_B)increases. Beyond a particular value of the external magnetic field, the energies begin to decrease and this behavior remains consistent across all considered cases when $m = n = 0$and$m = n = 1$. Figures 3(c) and 3(d) depict the magnetization plot against AB flux field (ζ_{AB})for varying external magnetic field(ω_B). The results show that magnetization decreases with increasing external magnetic field (ω_B)for $m = n = 0$and$m = n = 1$. Moreover, the magnitude of magnetization is higher when both AB flux and the external magnetic field are simultaneously present or at higher values in the system. Figures 4(a–d), display the magnetic susceptibility of the ARP at zero temperature under the combined influence of an external magnetic field and AB flux field. In Figures 4(a) and 4(b), the magnetic susceptibility is plotted against the external magnetic field (ω_B)for different AB flux field (ζ_{AB})values. The plots indicate that magnetic susceptibility decreases monotonically as the external magnetic field (ω_B) increases, particularly for $m = n = 0$and$m = n = 1$. In Figure 4(c), the magnetic susceptibility exhibits a nearly linear trend as the AB flux field (ζ_{AB}) increases for different values of the external magnetic field(ω_B). However, at low AB flux values, a sharp initial rise is observed before a gradual decline at higher flux values. Generally, the magnetic susceptibility decreases with increasing AB flux(ω_B)when$m = n = 0$. Figure 4(d) further examines the effect of the AB flux field (ζ_{AB}) on the zero-temperature of magnetic susceptibility for varying external magnetic field(ω_B). It is evident that the magnetic susceptibility first increases and reach a particular point before decreasing as the AB flux field (ζ_{AB}) increases, especially when$m = n = 1$.

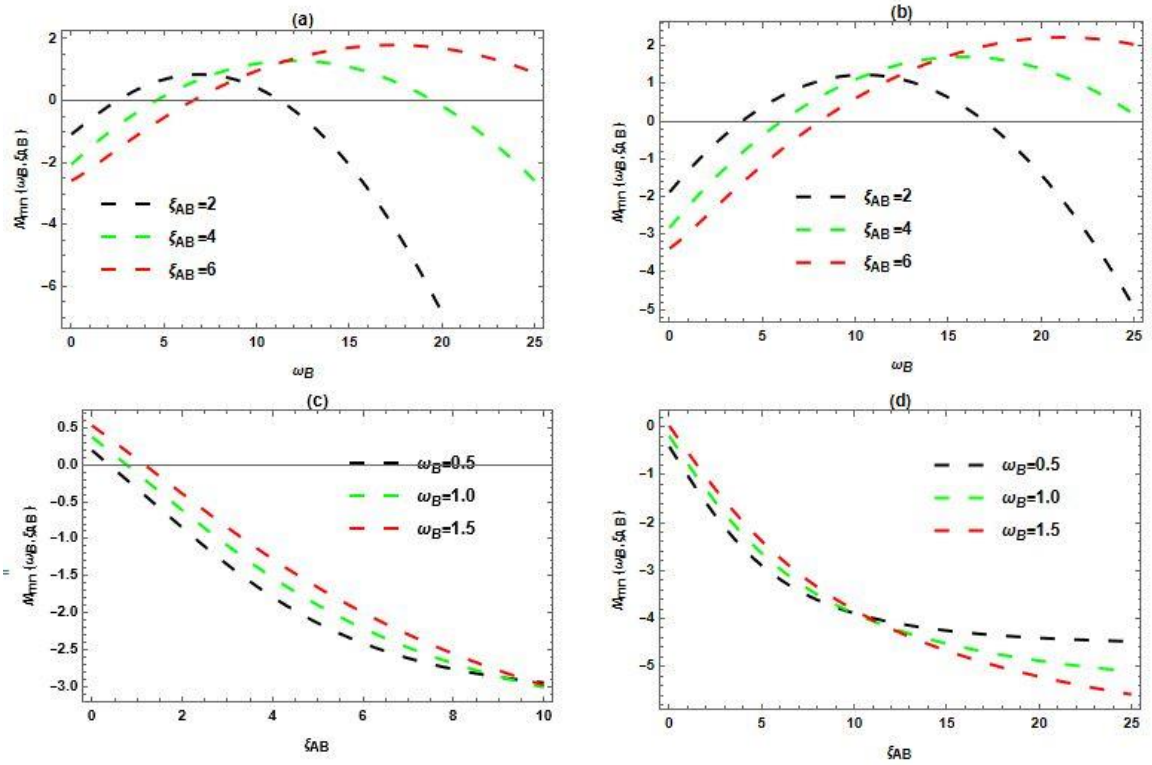

Figure 3: Plots of Magnetization at zero temperature against (a-b) External Magnetic Field ω_B varying AB flux ζ_{AB} andω_B. (c-d) AB flux ζ_{AB} varying ω_B

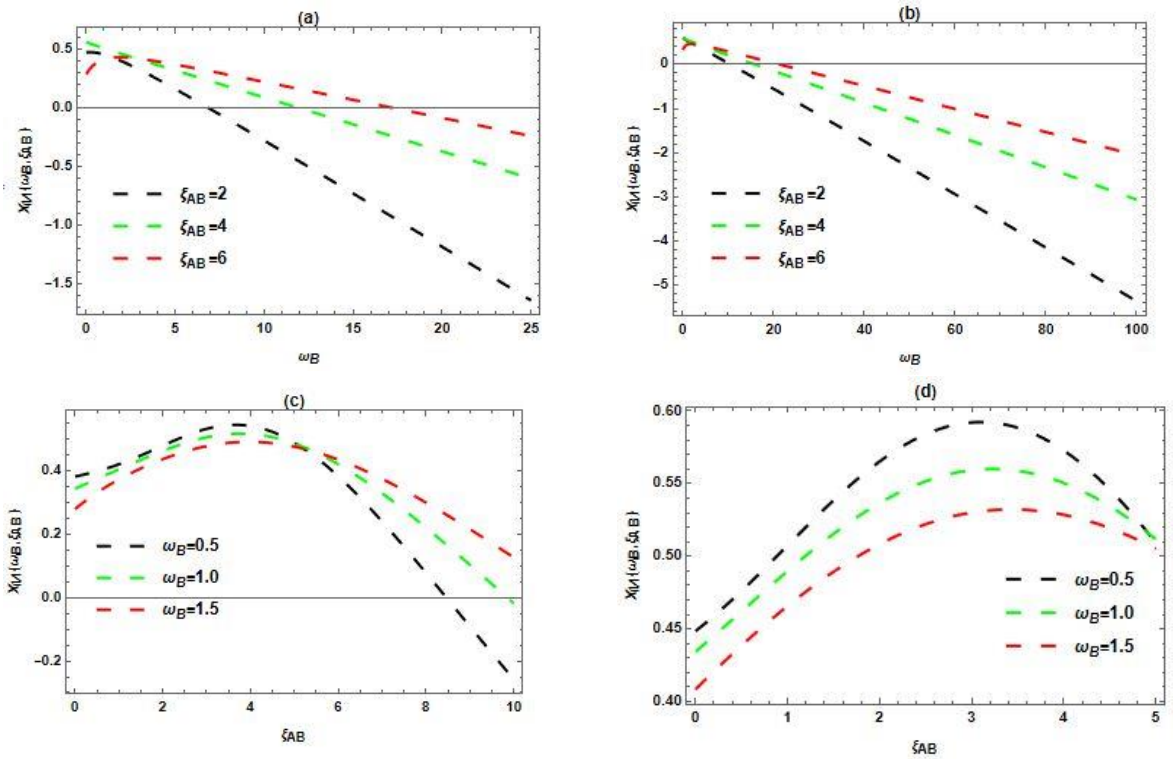

Figure 4: Plots of Magnetic Susceptibility at zero temperature against (a-b) External Magnetic Field ω_B varying AB fluxζ_{AB} andω_B. (c-d) AB flux ζ_{AB} varying ω_B ω_B

Partition function

Figures 5-9 present the graphical behavior of various thermodynamic quantities-namely the partition function, Helmholtz free energy, entropy, internal energy, and specific heat capacity of the Attractive Radial Potential (ARP) system under the influence of external magnetic and Aharonov-Bohm (AB) flux fields. In Figure 5(a), the partition function $Z(\omega_B, \zeta_{AB}, \beta)$ is plotted against the external magnetic field ω_B for a fixed value of the AB flux field ζ_{AB} at different temperaturesβ. The results reveal that the partition function increases monotonically with increasing external magnetic fieldω_B. Moreover, at higher temperatures$\beta = 0.06$, the partition function $Z(\omega_B, \zeta_{AB}, \beta)$ rises more significantly, showing that temperature enhances the statistical weight of accessible energy states when AB flux field ζ_{AB} is fixed. Figure 5(b) illustrates the variation of the partition function $Z(\omega_B, \zeta_{AB}, \beta)$ with the AB flux field $\zeta_{AB}$for a fixed value of external magnetic field ω_B varyingβ. The decreases in partition function $Z(\omega_B, \zeta_{AB}, \beta)$ due to the increased in AB flux fieldζ_{AB}, shows that the AB flux field attains to suppress the thermodynamic activity of the system. This trend is consistent within all temperature ranges considered, signifying that the AB field exerts a uniform moderating effect on the partition function.

Figure 5(c), shows the plot of partition function $Z(\omega_B, \zeta_{AB}, \beta)$ as a function of temperature β varying magnetic field strengths ω_B at a fixed AB flux fieldζ_{AB}. The plot revealed that the partition function $Z(\omega_B, \zeta_{AB}, \beta)$ increases steadily with temperature β in the region$2.0 < \beta < 3.0$, reflecting enhanced thermal excitations. However, beyond a certain temperature range$0.5 < \beta < 2.0$, the partition function becomes nearly constant, suggesting saturation of accessible energy states. Additionally, an increase in the magnetic field ω_B tends to reduce the partition function$Z(\omega_B, \zeta_{AB}, \beta)$, demonstrating the field's restraining effect on the system's thermodynamic response. Figure 5(d) depicts the dependence of the partition function $Z(\omega_B, \zeta_{AB}, \beta)$ on temperature $\beta$for different AB flux field ζ_{AB}values at a fixed magnetic fieldω_B. Initially, the partition function $Z(\omega_B, \zeta_{AB}, \beta)$ remains nearly constant with temperatureβ, but all the curves converge at a temperature$\beta = 0.6$, after which a simultaneous and pronounced increase in the partition function $Z(\omega_B, \zeta_{AB}, \beta)$ is observed. In the pseudoconstant region, the partition function $Z(\omega_B, \zeta_{AB}, \beta)$ is lower for higher AB flux values; however, beyond this region, it increases with risingζ_{AB}, indicating that at elevated temperatures, the AB flux field enhances the system's partition function.

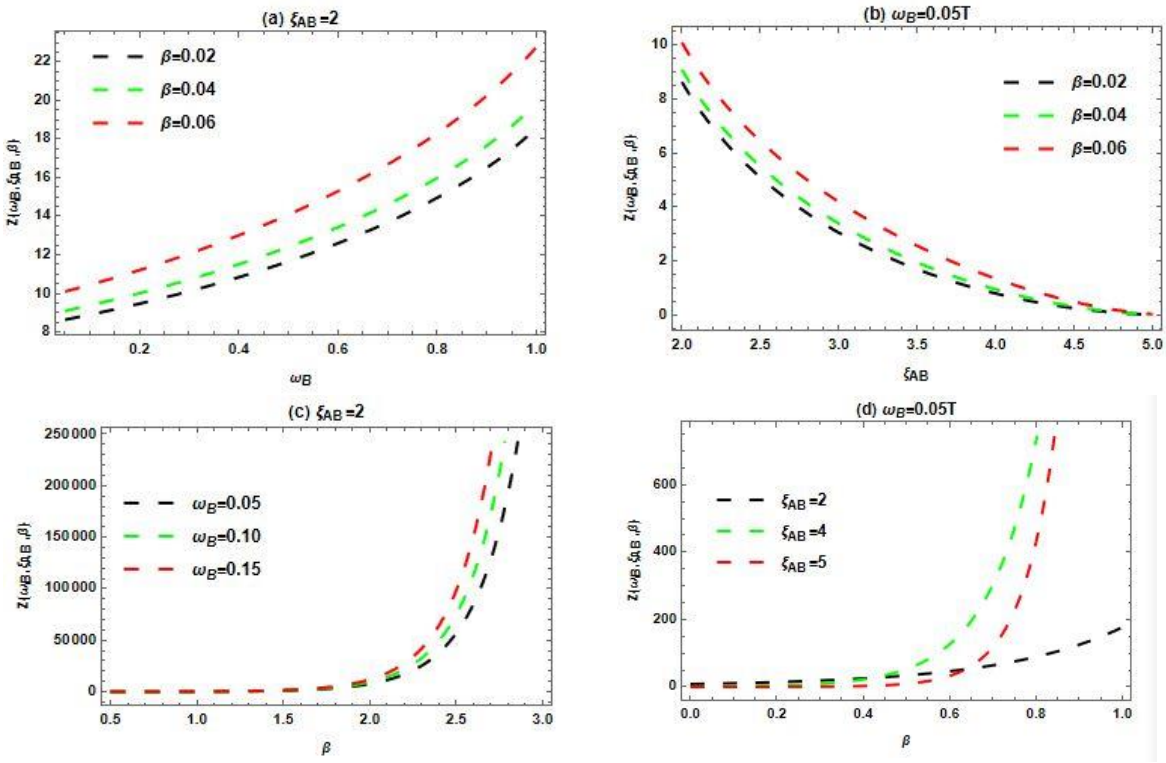

Figure 5: Plots of partition function $Z(\omega_B, \zeta_{AB}, \beta)$ as a function of (a) External Magnetic Field ω_B varying β (b) AB fluxζ_{AB} varying β (c) Temperature β varying ω_B (d) Temperature β varying ζ_{AB}

The Helmholtz free energy for the Attractive Radial Potential (ARP) system in the presence of Aharonov-Bohm (AB) flux and external magnetic fields is depicted in Figure 6. In Figure 6(a), the variation of Helmholtz free energy $F(\omega_B, \zeta_{AB}, \beta)$ with respect to the external magnetic field ω_B is shown for fixed values of the AB flux field ζ_{AB}at different temperaturesβ. The results indicate that free energy decreases as external magnetic field increases, implying that a stronger magnetic field reduces the system's available free energy, thereby lowering its thermodynamic potential. Figure 6(b) illustrates the dependence of the Helmholtz free energy $F(\omega_B, \zeta_{AB}, \beta)$ on the AB flux field $\zeta_{AB}$for fixed external magnetic field strengths ω_B while varying temperatureβ. It is observed that free energy increases progressively with increasing AB flux field, indicating that the AB flux enhances the system's stored energy and contributes to the rise in free energy.

In Figure 6(c), the Helmholtz free energy $F(\omega_B, \zeta_{AB}, \beta)$ is plotted against temperature β for different magnetic field values at a fixed AB flux. The free energy exhibits a steady, monotonic increase with temperature, suggesting that as the system gains thermal energy, its free energy grows correspondingly. A consistent influence of the magnetic field is observed for$\omega_B = 0.05T$, $\omega_B = 0.10T$ and$\omega_B = 0.15T$, showing that the external field uniformly affects the system's energetic response across the temperature range. Figure 6(d) shows the variation of Helmholtz free energy $F(\omega_B, \zeta_{AB}, \beta)$with temperature β for several AB flux field values at a fixed magnetic field. The plot reveals that free energy decreases with increasing temperature when $\zeta_{AB} = 4$and$\zeta_{AB} = 5$, while the free energy increases monotonically when$\zeta_{AB} = 2$. Furthermore, free energy is generally higher at stronger AB flux fields, even when the overall trend is declining. This behavior suggests that an intense AB flux field can significantly elevate the system's free energy. The observed decrease in free energy with temperature in some cases can be attributed to thermal disorder increases.

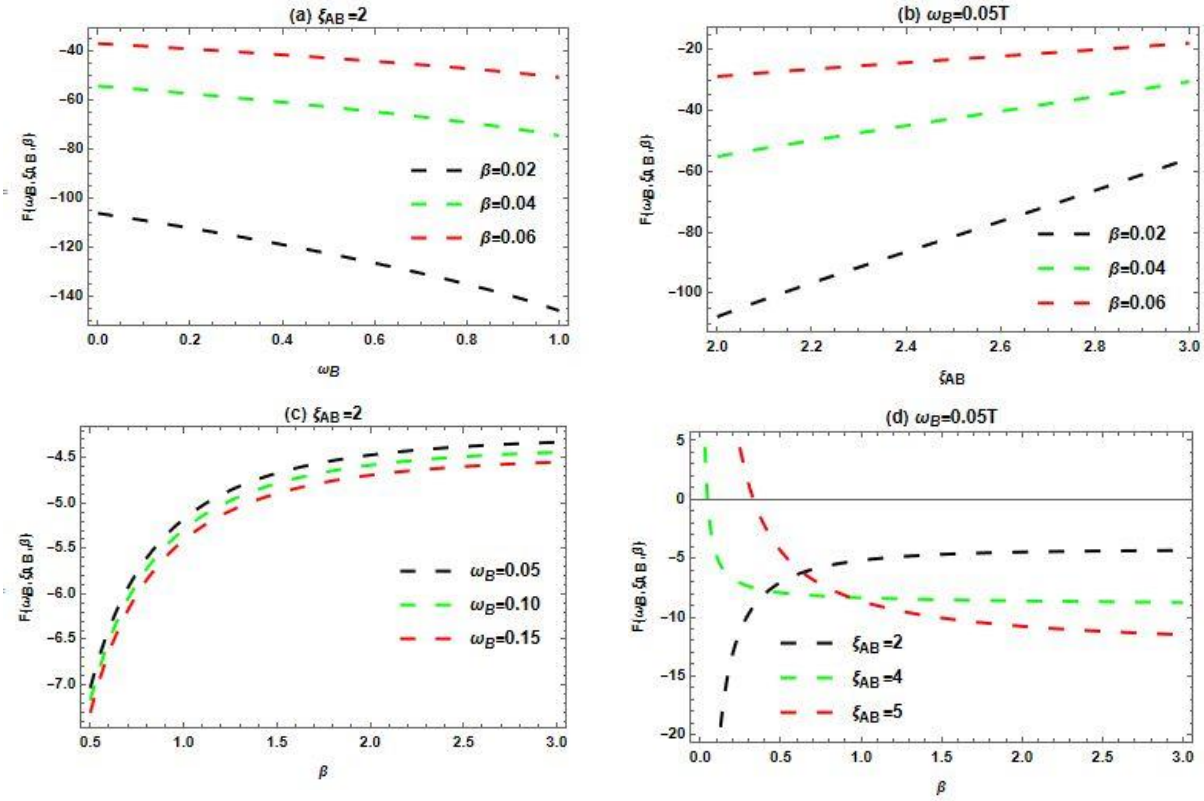

Figure 6: Plots of Helmholtz free energy $F(\omega_B, \zeta_{AB}, \beta)$ as a function (a) External Magnetic Field ω_B varying β (b) AB fluxζ_{AB} varying β (c) Temperature β varying ω_B (d) Temperature β varying ζ_{AB}

The entropy of the Attractive Radial Potential (ARP) system in the presence of external magnetic and Aharonov-Bohm (AB) flux fields exhibits a similar trend to that observed for the Helmholtz free energy, as shown in Figure 7. In Figure 7(a), the entropy $S(\omega_B, \zeta_{AB}, \beta)$ is plotted against the external magnetic field ω_B for fixed values of the AB flux field ζ_{AB}at different temperaturesβ. The plot reveals that entropy decreases with increasing magnetic field, indicating that a stronger magnetic field restricts the number of accessible microstates and reduces the degree of disorder in the system consistent with the behavior of the Helmholtz free energy. Figure 7(b) presents the variation of entropy $S(\omega_B, \zeta_{AB}, \beta)$with the AB flux field ζ_{AB}varying temperaturesβ at a fixed value ofω_B. The entropy of the system increases with increasing AB flux field, which indicate that the AB flux affects the system's configurational disorder and gives rise to greater thermodynamic behavior, showing the same trend in the free energy.

In Figure 7(c), entropy $S(\omega_B, \zeta_{AB}, \beta)$is plotted as a function of temperature β for a fixed AB flux field varying magnetic field. The entropy of the system depict a monotonically increase with temperature, indicating that higher thermal energy influence molecular agitation and disorder from the system. A uniform influence of the magnetic field is observed across the examined temperature range, similar to the consistent effect seen in the Helmholtz free energy plots. Figure 7(d) shows the variation of entropy $S(\omega_B, \zeta_{AB}, \beta)$with temperature for different AB flux field values at a fixed magnetic field. At lower temperatures, entropy decreases slightly with increasing temperature β at higher AB flux values but increases steadily for lower AB flux intensities. The overall pattern is analogous to that of the Helmholtz free energy, where an intense AB flux field amplifies both entropy and free energy. This similarity confirms the close thermodynamic relationship between the two quantities, as both are influenced by the combined effects of temperature, magnetic field, and AB flux in nearly identical ways.

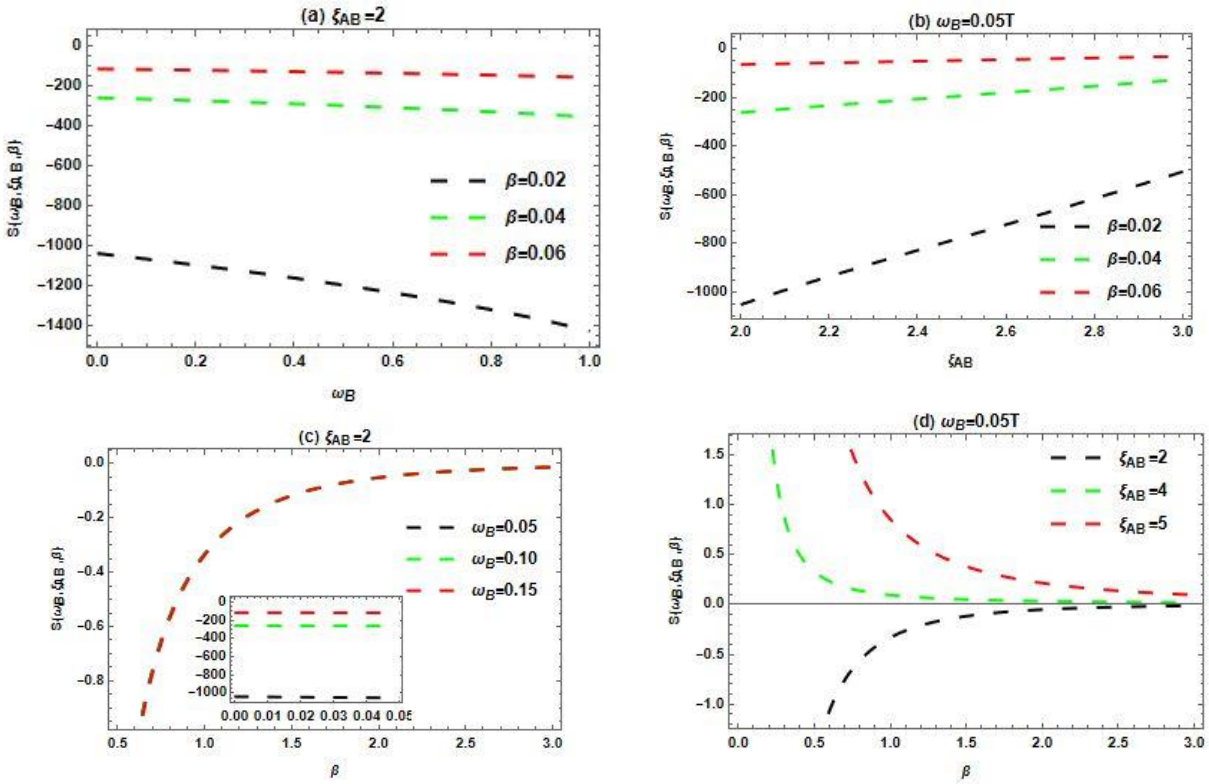

Figure 7: Plots of Entropy $S(\omega_B, \zeta_{AB}, \beta)$ as a function of (a) External Magnetic Field ω_B varying β (b) AB fluxζ_{AB} varying β (c) Temperature β varying ω_B (d) Temperature β varying ζ_{AB}

Figure 8 illustrates the variation of the internal energy of the Attractive Radial Potential (ARP) system under the combined influence of external magnetic and Aharonov-Bohm (AB) flux fields. In Figure 8(a), the internal energy $U(\omega_B, \zeta_{AB}, \beta)$ is plotted as a function of the external magnetic field ω_B for fixed values of the AB flux field ζ_{AB}at different temperaturesβ. The results show that internal energy decreases with increasing magnetic field, indicating that the application of a stronger magnetic field reduces the system's total internal energy due to the lowering of energy state occupancy. Figure 8(b) presents the variation of internal energy $U(\omega_B, \zeta_{AB}, \beta)$ with the AB flux field $\zeta_{AB}$for fixed external magnetic field $\omega_B$values while varying temperatureβ. It is observed that internal energy increases with increasing AB flux field, suggesting that the AB flux field enhances the energy levels of the system and contributes to higher internal energy values.

Figure 8(c), shows the plot of the internal energy $U(\omega_B, \zeta_{AB}, \beta)$ against temperature β for a different value of magnetic field, at constant AB flux field. The result depict that the internal energy decreases linearly with increasing temperature, which reveal that thermal excitation in the system contribute to a redistribution of energy levels within the possible available states, as a result in a gradual decline in the total internal energy of the system. The same behavior is observed across all the values of magnetic field consider, which indicates a consistency in thermal activity. Figure 8(d) shows the plot of the internal energy $U(\omega_B, \zeta_{AB}, \beta)$against temperature$\beta$ for different value of AB flux field at constant magnetic field. The plot demonstrates a steady decrease in internal energy as the temperature parameter βincreases. This relationship confirms that the internal energy diminishes at lower temperatures and is significantly influenced by the strength of the AB flux field.

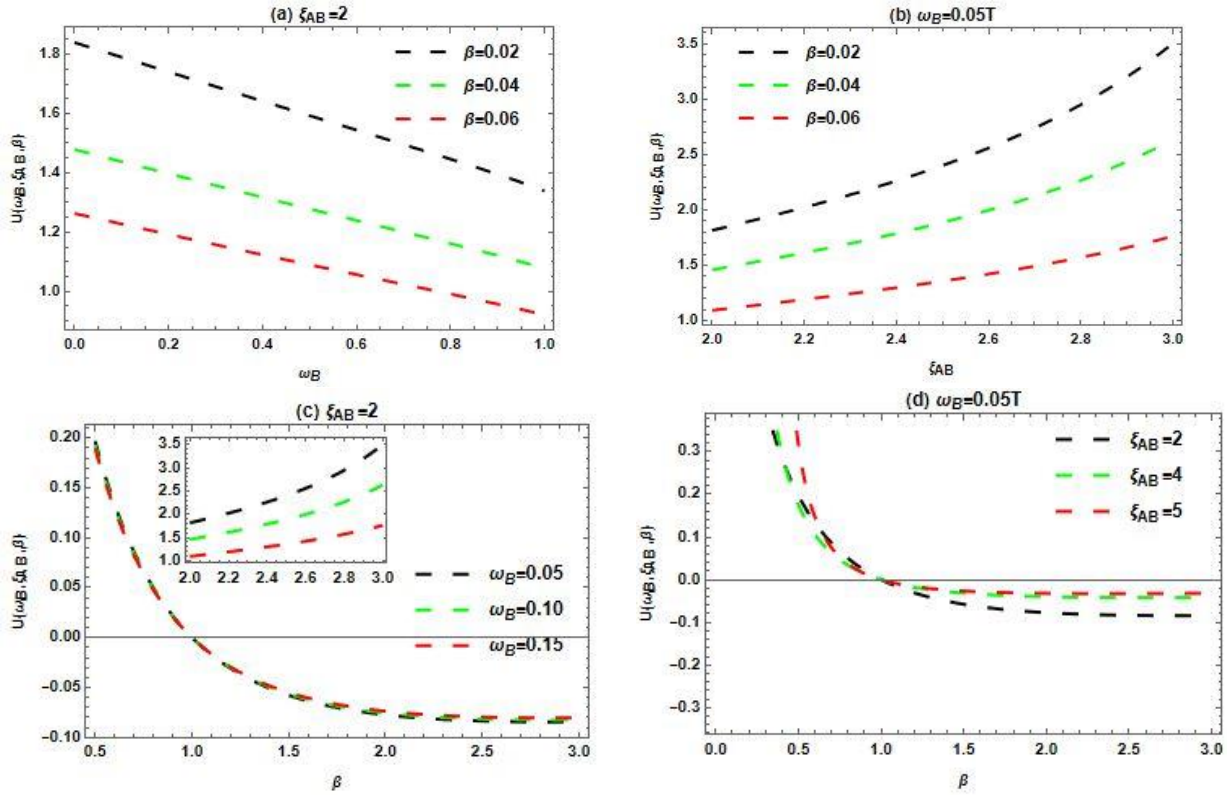

Figure 8: Plots of Internal Energy $U(\omega_B, \zeta_{AB}, \beta)$ as a function of (a) External Magnetic Field ω_B varying β (b) AB fluxζ_{AB} varying β (c) Temperature β varying ω_B (d) Temperature β varying ζ_{AB}

Figure 9 illustrates the specific heat capacity $C_v(\omega_B, \zeta_{AB}, \beta)$of the ARP system under the influence of both the Aharonov-Bohm (AB) flux and external magnetic fields. In Figure 9(a), the specific heat capacity is plotted against the external magnetic field for fixed values of the AB flux field at varying temperatures. The result shows that the specific heat capacity increases linearly with increasing external magnetic field. Figure 9(b) presents the variation of specific heat capacity with the AB flux field for fixed values of the external magnetic field at different temperatures. It is observed that the specific heat capacity decreases as the AB flux field increases. In Figure 9(c), the specific heat capacity is plotted as a function of temperature for different values of the external magnetic field while keeping the AB flux field constant. The plot reveals a monotonic increase in specific heat capacity with rising temperature. Similarly, Figure 9(d) shows the dependence of the system's specific heat capacity on temperature for different values of the AB flux field at a fixed external magnetic field. The specific heat capacity increases consistently with increasing temperature.

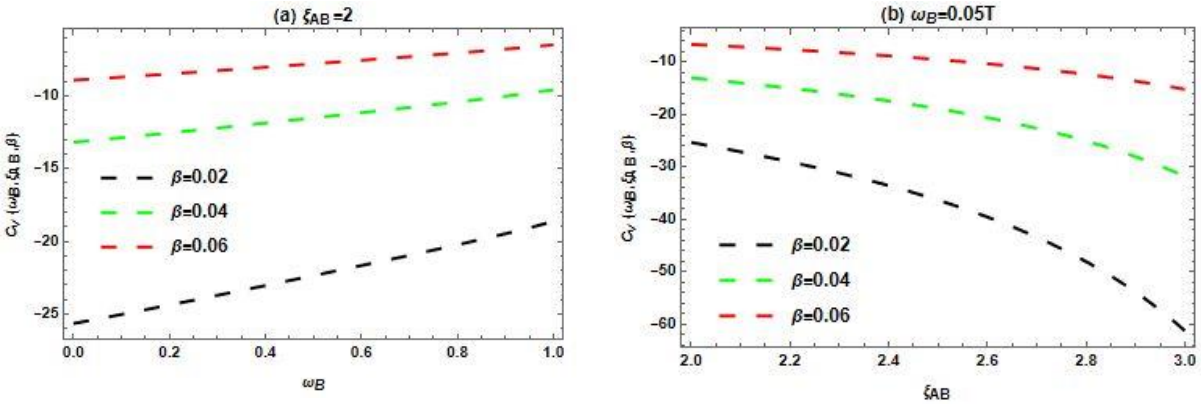

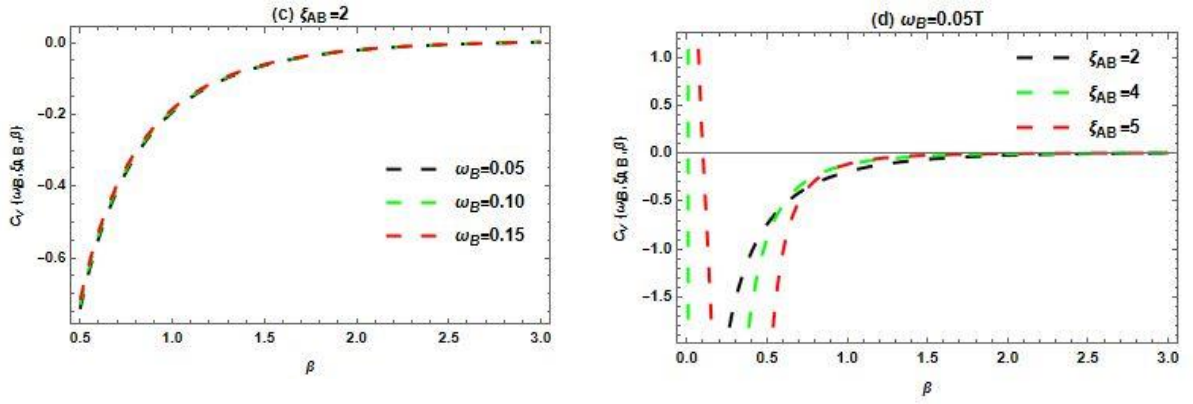

Figure 9: Plots of Specific heat capacity $C_v(\omega_B, \zeta_{AB}, \beta)$ as a function of (a) External Magnetic Field ω_B varying β (b) AB fluxζ_{AB} varying β (c) Temperature β varying ω_B (d) Temperature β varying ζ_{AB}

Magnetization and Magnetic Susceptibility at Finite Temperature

Figure 10 presents the plots of magnetization at finite temperature for the Attractive Radial Potential (ARP) system under the influence of external magnetic and Aharonov-Bohm (AB) flux fields. In Figure 10(a), the magnetization at finite temperature $M(\omega_B, \zeta_{AB}, \beta)$ is plotted against the external magnetic field ω_B for fixed values of the AB flux field ζ_{AB}at different temperaturesβ. The results show that $M(\omega_B, \zeta_{AB}, \beta)$ increases linearly with increasingω_B, indicating that the external magnetic field strengthens the magnetic response of the system due to enhanced spin alignment at finite temperature. Figure 10(b) depicts the variation of magnetization $M(\omega_B, \zeta_{AB}, \beta)$ with the AB flux field $\zeta_{AB}$for fixed external magnetic field ω_B at varying temperatureβ. The linear increase of$M(\omega_B, \zeta_{AB}, \beta)$ with increasingζ_{AB}, is observed. The result suggests that the AB flux field influence positively to magnetization of the system. This characteristics behavior is the same with the results obtained at zero temperature, to confirm the persistent effects of the AB flux field on magnetic behaviour of the.

In Figure 10(c), the magnetization at finite temperature$M(\omega_B, \zeta_{AB}, \beta)$ is plotted as a function of temperature β for different external magnetic field strengths ω_B at a fixed AB flux fieldζ_{AB}. The results reveal that $M(\omega_B, \zeta_{AB}, \beta)$ decreases with increasing temperatureβ, indicating that thermal agitation weakens magnetic ordering by randomizing spin orientations. Finally, Figure 10(d) shows the magnetization at finite temperature$M(\omega_B, \zeta_{AB}, \beta)$ as a function of temperatureβ for different AB flux field ζ_{AB}values at a fixed external magnetic fieldω_B. The plots demonstrate that $M(\omega_B, \zeta_{AB}, \beta)$ decreases with increasing temperatureβ for all ζ_{AB}values considered. This trend confirms that, although both the magnetic and AB flux fields enhance magnetization, thermal effects at higher temperatures tend to suppress it by reducing the degree of spin alignment within the system.

Figure 11 presents the plots of magnetic susceptibility at finite temperature for the Attractive Radial Potential (ARP) system under the influence of external magnetic and Aharonov-Bohm (AB) flux fields. In Figure 11(a), the magnetic susceptibility at finite temperature,$\chi_M(\omega_B, \zeta_{AB}, \beta)$, is plotted against the external magnetic field ω_B for fixed values of the AB flux field ζ_{AB}at different temperaturesβ. The results indicate that $\chi_M(\omega_B, \zeta_{AB}, \beta)$ decreases with increasing temperature, implying that thermal agitation weakens the system's magnetic response. However, at higher magnetic field, the system becomes saturated, which indicate a limited susceptibility beyond a certain value ofω_B. The result also reveals that the system predominantly indicates a paramagnetic property at $\chi_M(\omega_B, \zeta_{AB}, \beta) > 0$ within the range value ofω_B, consistent with the zero-temperature results. In the region$0.0T < \omega_B < 0.8T$ the results of the curves $\beta = 0.04$and$\beta = 0.06$ shows nearly constant pattern and a sharp increase is observed beyond$\omega_B = 0.8T$.

Figure 11(b) reveals the magnetic susceptibility $\chi_M(\omega_B, \zeta_{AB}, \beta)$ against AB flux field ζ_{AB}at constant values of the external magnetic field ω_B varying temperatureβ. The results shows that as ζ_{AB}increases,$\chi_M(\omega_B, \zeta_{AB}, \beta))$ decreases linearly, demonstrating that a stronger AB flux suppresses the magnetic response of the system. However, $\chi_M(\omega_B, \zeta_{AB}, \beta)$ increases with rising temperature, reflecting enhanced thermal contributions to magnetization. The system exhibits diamagnetic behavior for $\beta = 0.04$ and$\beta = 0.06$, while a slight paramagnetic tendency is observed at$\beta = 0.02$.

In Figure 11(c), the susceptibility $\chi_M(\omega_B, \zeta_{AB}, \beta)$ is plotted against temperature β for different external magnetic field strengths at a fixed AB flux fieldζ_{AB}. The plot shows that$\chi_M(\omega_B, \zeta_{AB}, \beta)$, decreases monotonically with increasing temperature, confirming that thermal

effects weaken the magnetization of the system. Similarly, the susceptibility decreases as ω_B increases, indicating that stronger magnetic fields tend to stabilize the spin orientations, thereby reducing the overall response. This variation of $\chi_M(\omega_B, \zeta_{AB}, \beta)$ with temperature reflects a diamagnetic behavior across the different ω_B values considered.

Finally, Figure 11(d) displays the magnetic susceptibility $\chi_M(\omega_B, \zeta_{AB}, \beta)$ as a function of temperature for different AB flux field values at a fixed external magnetic field. The results show that $\chi_M(\omega_B, \zeta_{AB}, \beta)$ increases gradually with temperature, while it decreases with increasing AB flux field strength. This inverse relationship between $\chi_M(\omega_B, \zeta_{AB}, \beta)$ and ζ_{AB}again indicates diamagnetic behavior, implying that the AB flux field opposes changes in the system's magnetic moment, particularly at higher flux intensities.

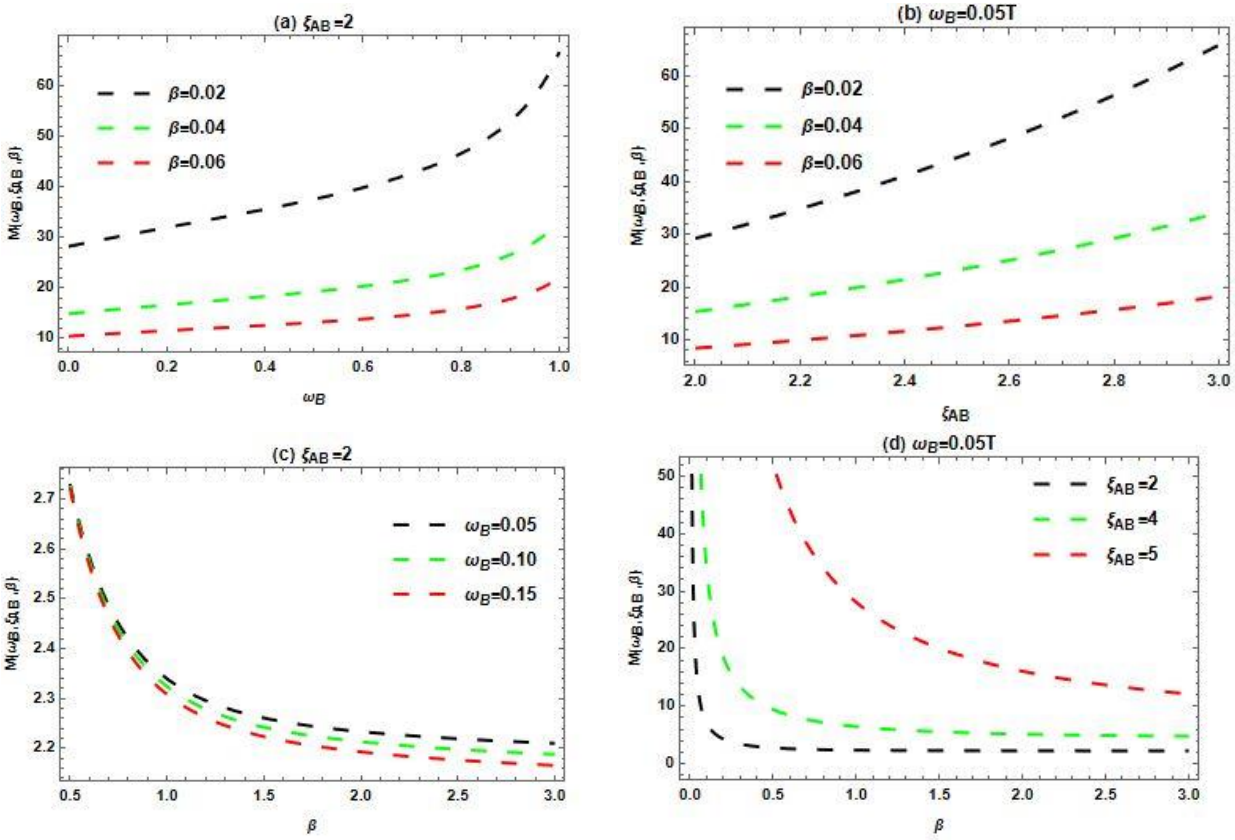

Figure 10: Plots of Magnetization at finite temperature $M(\omega_B, \zeta_{AB}, \beta)$ as a function of (a) External Magnetic Field ω_B varying β (b) AB fluxζ_{AB} varying β (c) Temperature β varying ω_B (d) Temperature β varying ζ_{AB}

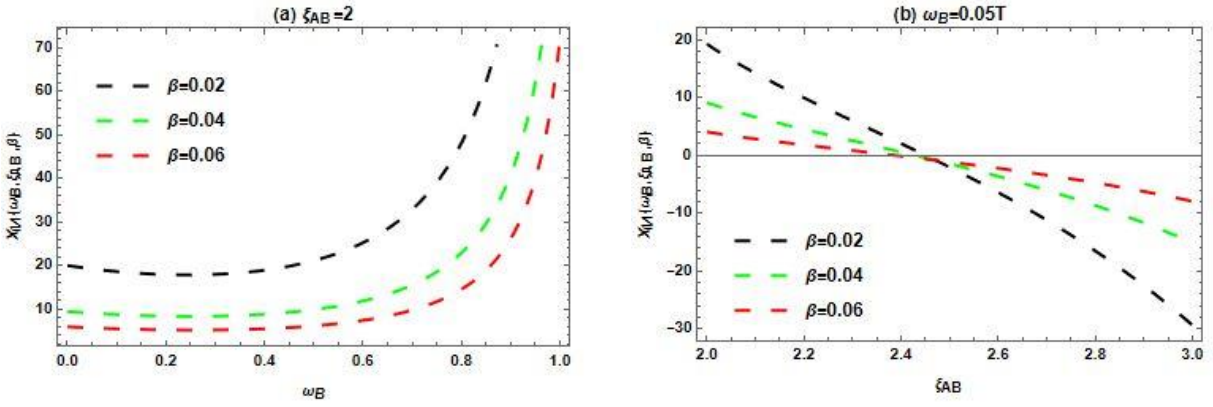

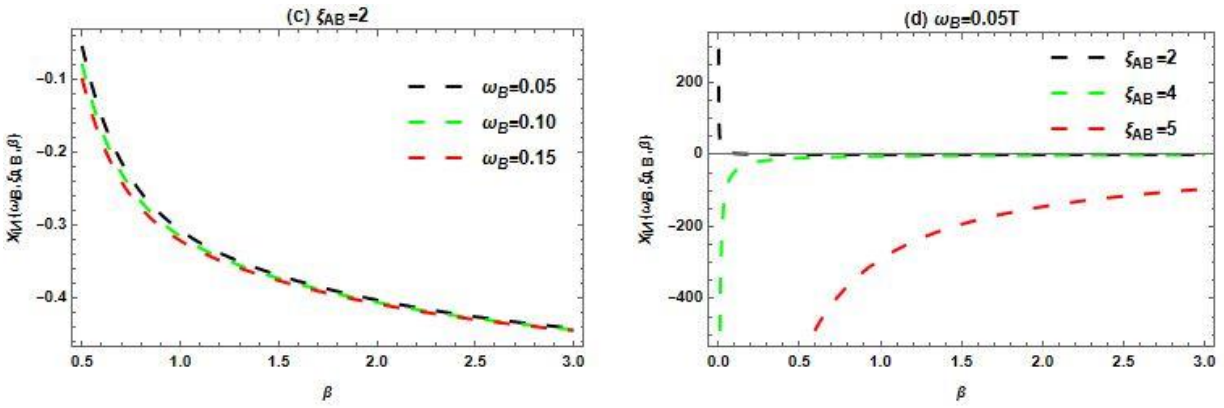

Figure 11: Plots of Magnetization at finite temperature $\chi_M(\omega_B, \zeta_{AB}, \beta)$ as a function of (a) External Magnetic Field ω_B varying β (b) AB fluxζ_{AB} varying β (c) Temperature β varying ω_B (d) Temperature β varying ζ_{AB}

CONCLUSION

In this research manuscript, we analytically solve the 2D non-relativistic Schrödinger equation for the Attractive Radial Potential (ARP) model influenced by Aharonov-Bohm flux and external magnetic fields using the Nikiforov-Uvarov Functional Analysis (NUFA) approach. Based on the derived energy eigenvalues, we further calculate key thermo-magnetic quantities such as free energy, internal energy, specific heat capacity, entropy, magnetization, and magnetic susceptibility.

Our result shows that the combine influence of the AB flux and magnetic field significantly affects energy spectrum of the system and its thermodynamic properties. The result also reveals that the energy eigenvalues decreases with an increase in AB flux and magnetic fields. The partition functions of the system and thermodynamic quantities show strong temperature response, for low temperatures value.

The free energy and entropy shows a uniform trend, by decreasing with increasing magnetic field and AB flux field strength. This trend suggests that the AB flux contribute to disorder and energy storage capacity in the system. The internal energy of the system decreases with temperature as well as magnetic field, confirming that higher external fields in the system enhance the accommodation of energy state in the system. Meanwhile, the specific heat capacity of the system also displays a peak value, behavior with discrete energy levels, which makes the transition between low- and high-temperature regimes.

Additionally, the investigation of magnetization and magnetic susceptibility shows that both quantities increase with magnetic field and AB flux but decrease with temperature due to thermal agitation. The system considers exhibits predominant paramagnetic properties at low AB flux and temperature turn to weak diamagnetism under high AB flux conditions. The results of this study can be extended to molecular physics (Okorie et al., 2021).

ACKNOWLEDGMENTS

We gratefully acknowledge the National Mathematical Centre, Abuja, for their contribution to the development of this research work.

REFERENCES

Abu-Shady, M. & Fath-Allah, H. M. (2023). The parametric generalized fractional Nikiforov-Uvarov method and its applications. *Eastern European Journal of Physics*. 3, 248–262.

Bayrak, O., Boztosun I and Ciftci, H. (2007). Exact Analytical Solutions to the Kratzer Potential by the Asymptotic Iteration Method," International Journal of Quantum Che- mistry, Vol. 107, No. 3, pp. 540-544. https://doi.org/10.1002/qua.21141

Çiftçi, H., Hall,R. L and Saad, N. (2005). Iterative solutions to the Dirac equation, Physics. Letter A 340, 388

Dirac, P. A. The Principles of Quantum Mechanics (Clarendon Press, Oxford, 1958).

Dong, S. H., *Factorization method in quantum mechanics* (Springer, Netherlands, 2007)

Edet, C.O., Amadi, P.O., Okorie, U.S., Tas, A., Ikot, A.N and Rampho, G. d (2020). Solutions of Schrodinger equation and thermal properties of generalized trigonometric Poschl-Teller potential, *Revista Mexicana de Fısica* 66 (6) 824–839 https://doi.org/10.31349/RevMexFis.65.333

Edet, C.O., Okoi, P. O., Yusuf, A. S., Ushie,P. O and Amadi, P. O (2020). Thermal properties and magnetic susceptibility of hellmann potential in Aharonov-Bohm (AB) flux and magnetic f ields at zero and finite temperatures. *Indian Journal of Physics* https://doi.org/10.1007/s12648-019-01650-0

Elsaid, M.K., Shaer, A., Hjaz, E. and Yahya, M.H. (2020) Impurity Effects on the Magnetization and Magnetic Susceptibility of an Electron Confined in a Quantum Ring under the Presence of an External Magnetic Field. *Chinese Journal of Physics*, 64, 9-17. https://doi.org/10.1016/j.cjph.2020.01.002

Eshghi, M and Hamzavi, M. (2012). Spin Symmetry in Dirac-Attractive Radial Problem and Tensor Potential, *Communication in theoretical physics*, 57, 355 https://doi.org/10.1088/0253-6102/57/3/05

Eshghi, M., Mehraban, H and Ikhdair, S. M. (2017). Approximate energies and thermal properties of a position-dependent mass charged particle under external magnetic fields, *Chinese Physics B* 26, 060302

Falaye, B. J., Sun, G. H., Ortigoz, R. S and Dong, S.H. (2016). Hydrogen atom in a Laser-Plasma, *Physics Review E* 93, 053201

Greene, R. L & Aldrich, C. (1976). Variational wave functions for a screened Coulomb potential *Physical Review A* 14, 2363 https://doi.org/10.1103/PhysRevA.14.2363

Greiner, W. Relativistic Quantum Mechanics: Wave Equations (Springer, Berlin, 2000).

Ikhdair, S. M and Falaye, B. J. (2014). Bound states of spatially dependent mass Dirac equation with the Eckart potential including Coulomb tensor interaction, The European Physical Journal Plus, 129.

Ikot, A. N., Edet, C. O., Amadi, P. O., Okorie, U.S., Rampho, G. J., and Abdullah, H. Y. (2020). Thermodynamic properties of Aharanov-Bohm (AB) and magnetic fields with screened Kratzer potential, European Physical Journal D 74 159 https://doi.org/10.1140/epjd/e2020-10084-9

Ikot, A. N., Okorie, U. S., Amadi, P. O., Edet, C. O., Rampho, G. J. and Sever, R. The Nikiforov–Uvarov-Functional Analysis (NUFA) Method: A New Approach for Solving Exponential-Type Potentials, *Few-Body System*. 62, 9 (2021)

Ikot, A.N., Rampho, G.J., Amadi, P.O., Sithole, M. J., Okorie, U.S and . Lekala, M. I. (2020). Theoretic quantum information entropies for the generalized hyperbolic potential, *Quantum Chemestry*, 120, 24 e26410 https://doi.org/10.1002/qua.26410

Karayer, H. (2020). Study of the radial Schrödinger equation with external magnetic and AB flux fields by the extended Nikiforov–Uvarov method, *European Physical Journal Plus* 135, 70

Karayer, H., Demirhan, D and Buyukkukih, F. (2015). Extension of Nikiforov-Uvarov method for the solution of Heun equation, *Journal of Mathematical Physics,* 56, 06350

Khordad, R. & Mirhosseini, B. (2015). Application of Tietz potential to study optical properties of spherical quantum dots. Pramana Journal of Physics, 85, 723–737

Koscik, P and Okopinska, A. (2007). Quasi-exact solutions for two interacting electrons in two-dimensional anisotropic dots, Journal of Physics A: Mathematical. Theory, 40 1045 (quant-ph/0607176).

Landau, L. D. E. & Lifshitz, M. Quantum Mechanics, Non- Relativistic Theory (Pergamon, New York, 1977).
Louis, H., Iserom, I. B., Akakuru, O. U., Nzeata-Ibe, N. A., Ikeuba, A. I., Magu, T. O., Amos, P. I.& Edet, C. O. (2018). I-state Solutions of the Relativistic and Non-Relativistic Wave Equations for Modified Hylleraas-Hulthen Potential Using the Nikiforov-Uvarov Quantum Formalism, *Oriental Journal of Physical Science.* 03,(1) 03-09

Nikiforov, A. F and Uvarov, V. B. *Special functions of mathematical physics* (Birkhauser, Basel, 1988)

Okorie, U. S.; Ikot, A. N.; Onate, C. A.; Onyeaju, M. C.; Rampho, G. J. (2021). Bound and scattering states solutions of the Klein-Gordon equation with the attractive radial potential in higher dimensions, *Modern Physics Letter A* 36, No. 32, Article ID 2150230, 15 p.

Okorie, U.S., Ikot, A.N and Chukwuocha, E. O. (2019). The Statistical Properties of The Varshni Potential Model Using Modified Factorization Method, *Scientia Africana*, Vol. 18 (No. 3), Pp 47-60

Okorie, U.S., Edet, C.O., Ikot, A.N., Rampho G. J. and Sever, R. (2020). Thermal Properties of Deng-Fan-Eckart Potential model using Poisson Summation Approach, *Journal of Mathematical Chemistry*. 58, 989 https://doi.org/10.1007/s10910-020-01107-4

Pekeris, C. L. (1934). The Rotation-Vibration Coupling in Diatomic Molecules *Physical Review*. 45, 98 https://doi.org/10.1103/PhysRev.45.98

Qiang, W. C and Dong, S. H. (2010). Proper quantization rule, *Europhysics Letters*. 89, 10003. https://doi.org/10.1209/0295-5075/89/10003

Schiff, L. I. Quantum Mechanics (McGraw Hill, New York, 1995).

Serrano, F. A., Xiao-Yan G., & Shi-Hai D. (2010). Qiang-Dong proper quantization rule and its applications to exactly solvable quantum systems. *Journal of Mathematical Physics* 51, 8, 082103

Serrano, F. A., Cruz-Irisson, M and Dong, S. H. (2011). Proper quantization rule as a good candidate to semiclassical quantization rules, *Annalen der Physik*, 523, 771-782

Servatkhah, M., Khordad, R., Firoozi, A., Rastegar Sedehi, H. R. & Mohammadi, A. (2020). Low temperature behavior of entropy and specific heat of a three dimensional quantum wire: Shannon and Tsallis entropies. *European Physical Journal B* 93, 1–7

Servatkhah, M., Khordad, R and Ghanbari, A. (2020). Accurate Prediction of Thermodynamic Functions of H_2 and LiH Using Theoretical Calculations, *International Journal of Thermophysics.* 41, 37

Williams, B. W and Poulios, D. P. (1993). A simple method for generating exactly solvable quantum mechanical potentials, European Journal of Physics, 14, 222 https://doi.org/10.1088/0143-0807/14/5/006